JACS
JOURNAL OF THE AMERICAN CHEMICAL SOCIETY
pubs.acs.org/JACS
Article

Long-Range Electrostatic Colloidal Interactions and Specific Ion Effects in Deep Eutectic Solvents

Adrian Sanchez-Fernandez,* Andrew J. Jackson, Sylvain F. Prévost, James J. Doutch, and Karen J. Edler

Cite This: J. Am. Chem. Soc. 2021, 143, 14158−14168
Read Online
ACCESS | Metrics & More | Article Recommendations | Supporting Information

ABSTRACT: While the traditional consensus dictates that high ion concentrations lead to negligible long-range electrostatic interactions, we demonstrate that electrostatic correlations prevail in deep eutectic solvents where intrinsic ion concentrations often surpass 2.5 M. Here we present an investigation of intermicellar interactions in 1:2 choline chloride:glycerol and 1:2 choline bromide:glycerol using small-angle neutron scattering. Our results show that long-range electrostatic repulsions between charged colloidal particles occur in these solvents. Interestingly, micelle morphology and electrostatic interactions are modulated by specific counterion condensation at the micelle interface despite the exceedingly high concentration of the native halide from the solvent. This modulation follows the trends described by the Hofmeister series for specific ion effects. The results are rationalized in terms of predominant ion−ion correlations, which explain the reduction in the effective ionic strength of the continuum and the observed specific ion effects.

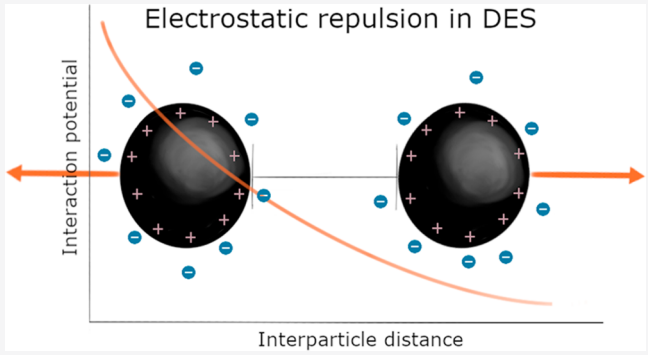

INTRODUCTION

Electrostatic interactions play an essential role in biological and technological processes. From ion motion in batteries to protein function in living cells, charge modulation dictates the function of processes that involve ions.[1,2] The classical approach to treat electrostatics considers ions as ideal point charges, where no ion−ion interactions occur as ions with no volume are considered to exist in a theoretically dilute regime.[3] To account for the nonidealities arising from electrostatic forces between ions, Debye and Hückel formulated the theory that describes the interaction landscape in dilute electrolytes by adding an activity coefficient that quantifies such an interaction.[4] Subsequently, DLVO theory was developed to quantitively describe the interplay between van der Waals attraction forces and electrostatic repulsion in colloidal systems.[5] Although DLVO theory has been the benchmark framework to describe colloidal stability, it is well-known that electrostatics are driven not only by the ion charge but also by other complex mechanisms, e.g. the solvation free energy of the ions near macromolecules, specific charge−charge interactions, and Hofmeister effects.[6] However, all these theories fail to accurately describe important biological and technological processes, as electrostatic interactions in concentrated ion solutions are far from the ideal behavior.[7] Recent investigations have shown that ion−ion correlations at high ion concentrations, such as in concentrated electrolytes and ionic liquids, reduce the apparent ionic strength of the continuum.[8,9] This prompts complex ionic systems to show a reversion in the Debye−Hückel theoretical predictions, and larger Debye lengths are observed with increasing ion concentrations at high ionic strength.

Deep eutectic solvents (DES) are sustainable liquids obtained and stabilized through the formation of an extensive hydrogen bond network often between an organic salt with a neutral molecule at a eutectic ratio specific to the mixture (e.g., 1 mol of choline chloride:2 mol of urea).[10−12] The result from the complexation of the precursors is a solvent at room temperature. DES are promising sustainable alternatives to traditional molecular solvents in a variety of applications. For instance, these solvents have been proposed as environments for protein preservation, metal electrodeposition, and synthesis of nanostructured materials and as electrolytes in green lithium-ion batteries, among others.[13−17] All of these applications share a common theme; i.e. electrostatics dictate the behavior of the systems. The theoretical ionic strength of DES is often higher than 2.5 M when all ions are assumed to be dissociated. Under these conditions, the predicted Debye length becomes no larger than the ion radius. Thus, long-range electrostatic interactions should be completely screened at these ion concentrations.[9] However, DES may present another

Received: May 8, 2021
Published: August 30, 2021

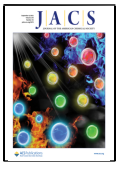

https://doi.org/10.1021/jacs.1c04781
J. Am. Chem. Soc. 2021, 143, 14158−14168

exception to the traditional framework for electrostatic interactions, as occurs with ionic liquids and other concentrated electrolytes. Thus, investigating the electrostatic interaction landscape in DES is of great relevance for understanding and developing better technologies based on these solvents and will also contribute to the development of knowledge about highly ionic systems.[8]

Small-angle scattering provides one of the very few methods that allows a direct probe of the correlations between colloidal particles (e.g., micelles). As such, modeling approaches have been developed to probe interaction potentials. Hard-sphere (HS) or Coulomb interaction potentials can be modeled from small-angle scattering data of concentrated samples, and the strength and decay profile of the interaction potential can be investigated.[18−22] In this paper, we present an investigation of long-range interparticle interactions in DES. Also, the modulation of electrostatic forces due to the condensation of different counterions at the particle interface was probed. To probe colloidal interactions in DES, we measured the scattering from dodecyltrimethylammonium ($C_{12}TA^+$) micelles with different counterions (chloride, Cl^-; bromide, Br^-; nitrate, NO_3^-; and sulfate, SO_4^{2-}) at different volume fractions in 1:2 choline chloride:glycerol and 1:2 choline bromide:glycerol. The behavior of these surfactants has been extensively studied in aqueous solution and ionic liquids, thus providing a baseline comparison to the results presented here. Also, the results were compared to the theoretical predictions for hard spheres interacting through excluded volume effects.

EXPERIMENTAL SECTION

Materials. Protiated choline bromide (h-ChBr, TCI Chemicals, >98%), protiated glycerol (h-Glyc, Sigma-Aldrich, 99%), deuterated choline chloride (d-ChCl, CK Isotopes, 99%, 99.6% D), deuterated glycerol (d-Glyc, CK Isotopes, 99%, 99% D), protiated $C_{12}TAC$ (h-$C_{12}TAC$, Sigma-Aldrich, >99%), protiated $C_{12}TAB$ (h-$C_{12}TAB$, Sigma-Aldrich, 99%), and D_2O (Sigma-Aldrich, 99.9% D) were purchased and used as received. Protiated 1:2 choline bromide:glycerol (h-ChBr:h-Glyc) and deuterated 1:2 choline chloride:glycerol (d-ChCl:d-Glyc) were prepared following the same protocol presented for the synthesis of protiated 1:2 choline chloride:glycerol.[12] Solvents were freeze-dried, sealed, and stored under a dry atmosphere to minimize water absorption. Water content was determined using a Mettler-Toledo DL32 Karl Fischer titrator to an average content of 0.32 and 0.64 wt % for the chloride- and bromide-based solvents respectively, during the experimental procedure presented here.

Protiated $C_{12}TANO_3$ (h-$C_{12}TANO_3$) and $C_{12}TA(SO_4)_{1/2}$ (h-$C_{12}TA(SO_4)_{1/2}$) were prepared by exchanging the chloride counterion from $C_{12}TAC$ following the procedure presented in the Supporting Information (SI).[23] Tail-deuterated dodecyltrimethylammonium bromide (d-$C_{12}TAB$, d_{25}) was prepared at the ISIS Deuteration Facility and used as received.

Samples for small-angle neutron scattering (SANS) measurements were prepared by dilution of stock solutions of the different surfactants in each solvent. Stock solutions were prepared by directly mixing each surfactant in the DES and equilibrated at 50 °C for 24 h. These stock solutions were diluted using pure DES to reach the desired final concentrations. The samples were equilibrated at 50 °C for 24 h, sealed, and stored under a dry atmosphere to prevent water adsorption. Samples in D_2O were prepared using the same protocol without requiring the equilibration step.

Methods. SANS experiments were performed on Sans2d (ISIS Pulsed Neutron Source, UK)[24] and D11 (Institute Laue-Langevin, France).[25] For both experiments, samples were loaded in 1 mm path length, 1 cm width, quartz Hellma cells. The cells were placed in a temperature-controlled sample changer at a constant temperature of 50 °C during measurement for the samples containing surfactants in DES. Surfactant samples in D_2O were measured at 25 °C. Data reduction was performed using the standard protocols of each beamline accounting for sample transmission, detector efficiency, and the scattering from an empty cell, and resulting in data sets containing the absolute scattered intensities, $I(q)$ in cm^{-1}, versus momentum transfer, q in $Å^{-1}$.[26,27] The scattering of the solvents was subtracted as a background contribution accounting for the incoherent scattering from each sample. The theoretical models were smeared using a Gaussian function to account for instrument resolution.[28]

SANS data analysis was performed using a model-based approach. The small angle scattered intensity from an isotropic, centrosymmetric particle can be written as

$$I(q) = \phi_p V_p (\Delta SLD)^2 P(q) S'(q) \quad (1)$$

where ϕ_p is the volume fraction of particles, V_p is the particle volume, and ΔSLD is the difference in the scattering length density (SLD) between particles and the solvent. The form factor, $P(q)$, and the apparent interparticle structure factor, $S'(q)$, are q-dependent functions that respectively describe the particle morphology and interparticle interactions. Previous investigations on the micellization of alkyltrimethylammonium bromide surfactants in choline chloride:glycerol DES have shown that the SANS data from micelles in the dilute regime can be satisfactorily modeled using a uniform ellipsoid form factor.[29,30] As such, we have decided to use this model to account for the form factor of the micelles. The analytical model uses two structural parameters to describe the shape of the uniform ellipsoid, the equatorial radius perpendicular to the rotation axis of the spheroid, r_{eq}, and the aspect ratio between the two radii of the spheroid, AR (AR = r_{po}/r_{eq}, where r_{po} is the polar radius parallel to the rotational axis of the spheroid). When AR > 1, this model describes an ellipsoid with a prolate distribution of mass.

The SLD of each component of the system was calculated by accounting for the neutron scattering length of the atomic group (Σb_i) and the volume this occupies (V_m). As the solvation of the headgroup and the chemical similarity between the quaternary ammonium headgroup and solvent components significantly reduces the scattering contribution of the headgroup region,[29] the scattering signal is dominated by the micelle core for the isotopic mixtures used in these experiments. Therefore, the SLD of the micelle was calculated as equivalent to that of the lyophobic tail and fixed during fitting, neglecting possible solvation in the core by the DES. Molecular volumes, neutron scattering lengths, and SLDs used for the analysis of the data are presented in Table 1.

Table 1. Volumes, Neutron Scattering Lengths, and Scattering Length Densities of the Constituents of the Systems Studied Here

Unit	V_m/Å^3	$\sum b_i$/fm	SLD/×10^{-6} Å^{-2}
d-ChCl:d-Glyc	434.9	281	6.40
h-ChBr:h-Glyc	434.9[a]	17.7	0.42
$C_{12}D_{25}$	350.2[b]	242	6.92
$C_{12}H_{25}$	350.2[b]	−13.7	−0.39
D_2O	30.07	19.1	6.37

[a]The molecular volume of 1:2 choline bromide:glycerol has been approximated as the same as that of the 1:2 choline chloride:glycerol.[29] This is a reasonable assumption based on the similar size of the anions (r_{Cl} = 181 pm; r_{Br} = 196 pm).[31] [b]The molecular volume of the surfactant tail was calculated using the Tanford equations.[32]

The dynamic character of micellization is expected to follow a rapid association−dissociation equilibrium, as it does in aqueous solution. This results in a population of micelles with different aggregation numbers, which is predicted to follow a relatively narrow distribution for globular aggregates.[29,33] A polydispersity function (p) was included to account for the nonuniformity of the micelles. The size distribution was implemented using a Schulz distribution.[34] The

https://doi.org/10.1021/jacs.1c04781
J. Am. Chem. Soc. 2021, 143, 14158−14168

distribution was parametrized for both equatorial and polar radii using $z = 5.6$, $N_{pts} = 80$, and $N_\sigma = 8$, where z is the width of the distribution, N_{pts} is the number of points used to compute the function, and N_σ defines how far into the tails the distribution is considered in the calculation. This gives a polydispersity value of 0.15, which is a common value for structural fluctuations in globular micelles.[33] Small variations of this parameter (±0.05) did not show significant variations in the results from the fits.

As the morphology of dodecyltrimethylammonium halide micelles remains rather unchanged with surfactant concentration in 1:2 choline chloride:glycerol,[29] the experimental structure factor can be deconvoluted from the data using the known form factor (from, e.g., particle structure in the dilute regime) using eq 2:

$$S'(q) = \frac{I(q)}{KP(q)} \tag{2}$$

where K is a factor that accounts for the particle concentration and contrast factor. As such, the experimental structure factor can be extracted and fitted using mathematical models that describe the interactions between particles.

The structure factor for spherical particles, $S(q)$, has been analytically derived for different interaction potentials. The hard sphere (HS) model accounts for the correlation between particles interacting through excluded volume effects. This model is described using two parameters: the effective radius of the particle, r_{eff}, and the volume fraction of particles, ϕ_p, with a resulting number density, n, that matches that of the micelles and defined as

$$n = \frac{3\phi_p}{4\pi r_{eff}^3} \tag{3}$$

The interaction potential, $v(r)$, at an interparticle distance r is calculated using the following closure relation to resolve the Ornstein–Zernike equation, where r is the center-to-center distance between particles:[18,35]

$$v(r)_{HS} = \begin{cases} \infty, & r < 2r_{eff} \\ 0, & r > 2r_{eff} \end{cases} \tag{4}$$

This model has been successfully applied to account for the interaction between uncharged particles or those with screened electrostatic interactions.[36,37]

The interaction component in the scattering for charged colloidal particles can be calculated using the rescaled mean spherical approximation (RMSA), a rework of the original mean spherical approximation derived by Hayter and Penfold to describe interactions at low particle volume fractions using the Yukawa potential.[19,20] This model describes electrostatic interactions between charged hard spheres in an electrolyte solution of ionic strength I and uses the following closure relationship to calculate the interaction potential from the Ornstein–Zernike equation:

$$v(r)_{RMSA} = \begin{cases} \infty, & r < 2r_{eff} \\ 4\pi \in_0 \in r_{eff}^2 \psi_0^2 \exp(-\kappa(r - 2r_{eff}))/r, & r > 2r_{eff} \end{cases} \tag{5}$$

where ε_0 and ε are the vacuum permittivity and solvent relative permittivity, k_B is the Boltzmann constant, T is the system temperature, ψ_0 is the particle surface potential, and κ is the inverse of the Debye screening length, which is given by eq 6:

$$\kappa = \sqrt{\frac{2N_A e^2 I}{\in_0 \in k_B T}} \tag{6}$$

where N_A is Avogadro's number, e is the electron charge, and I is the ionic strength of the solution. Using the macroion charge, z_p, the surface potential is calculated as

$$\psi_0 = \frac{z_p e}{4\pi \in_0 \in r_{eff}(1 + \kappa r_{eff})} \tag{7}$$

The reduced potential for the mean interparticle spacing, a, allows for determination of the Coulomb coupling constant, Γ_k, from the fitting results using the eq 8:

$$\Gamma_k = \frac{2v(r = 2a)_{RMSA}}{k_B T} \tag{8}$$

And the mean interparticle spacing is approximated using[19]

$$a = \left(\frac{3}{4\pi n}\right)^{1/3} \tag{9}$$

which combined with eq 3 gives

$$a = \frac{r_{eff}}{(\phi_p)^{1/3}} \tag{10}$$

Note that the surface-to-surface distance between particles is given by $a - 2r_{eff}$. The dimensionless Coulomb coupling constant, Γ_k, relates to the strength of the electrostatic force exerted between particles separated by an arbitrary interparticle distance, r. This interparticle distance is conveniently defined as $r = 2a$ and can be used to quantify electrostatic interactions within a colloidal dispersion. Further details in the derivation of the interaction potential can be found in the original reports.[19,20]

The $S(q)$ models presented above (eqs 4 and 5) are derived for interacting spherical particles. However, the interpretation of scattering data from nonspherical particles is complicated by the shape- and orientation-dependent interaction, thus, resulting in inaccurate $S(q)$ models for anisotropic particles. The decoupling approximation (DA) was developed to correct the scattering contribution from the interaction of nonspherical and polydisperse particles.[34] This approach assumes that there is no correlation between particle position and orientation, and it has been proved a reasonable approximation for moderately anisotropic and polydisperse particles.[38,39] The apparent interparticle structure factor is formally defined as

$$S'(q) = 1 + \beta(q)[S(q) - 1] \tag{11}$$

$$\beta(q) = \frac{|\langle F(q)\rangle|^2}{\langle |F(q)|^2\rangle} \tag{12}$$

where $F(q)$ is the amplitude of the form factor and $S(q)$ is the analytical structure factor for interacting spheres. The effective radius used to calculate the $S(q)$ is defined as the radius of a spherical particle with the same second virial coefficient as the colloidal particles. This is determined for ellipsoids using eq 13:

$$r_{eff} = (r_{eq}^3 AR)^{1/3} \tag{13}$$

A systematic approach has been followed to analyze the SANS data presented here. Initially, the micelle form factor was determined from the micellar scattering in the dilute regime, and eq 2 was used to extract the experimental structure factor from higher surfactant concentrations. The parameters r_{eff} and $\beta(q)$ were calculated from the fitted $P(q)$ (eqs 12 and 13) and those were fixed during the analysis of the $S'(q)$ data. The Coulomb coupling factor was used to parametrize the apparent structure factor models using the RMSA. Due to the correlation of the Debye length, of which the ionic strength of the solvent is unknown, and the particle surface potential (eq 5, 6 and 7), no specific values of the ionic strength or particle charge could be directly calculated. The results from the modeling of $S'(q)$ were subsequently convoluted with the particle form factor, and the resulting $P(q)\cdot S'(q)$ models were validated against the experimental data.

Model-based analysis of the SANS data was performed using SasView 5.0.3, and the experimental data were fitted using the nonlinear least-squares method Levenberg–Marquardt algorithm. For

https://doi.org/10.1021/jacs.1c04781
J. Am. Chem. Soc. 2021, 143, 14158–14168

further information on the definition of the mathematical models and functions, refer to the original references and the SasView documentation.[40]

RESULTS

The scattering of h-C_{12}TAC in 1:2 d-ChCl:d-Glyc was initially measured at different surfactant concentrations, and these concentrations were decided based on previous investigations. The lowest concentration (78.8 mM) was selected to be in the dilute regime, where interparticle scattering is negligible, while still giving a good signal-to-noise ratio.[29] The concentrated samples were measured up to a concentrated micellar phase (1070 mM), defined to be below the transition to lyotropic phases.[41,42] As the form factor of the micelles remains unchanged in the concentration range investigated here (See Figure S1 and Table S1), the apparent structure factor, $S'(q)$, was deconvoluted. The scattering from different concentrations of C_{12}TAC in D_2O was measured and treated using the same approach. The deconvoluted $S'(q)$ and best fits using the RMSA model are presented in Figure 1, together with the main results from the analysis.[19,43] The fits to the experimental scattering data are included in Figure S1, and the results from the analysis are presented in Table S1. The relative static permittivities used for the structure factor calculations are ε_{DES} = 22.8 and ε_{D2O} = 77.9.[44,45]

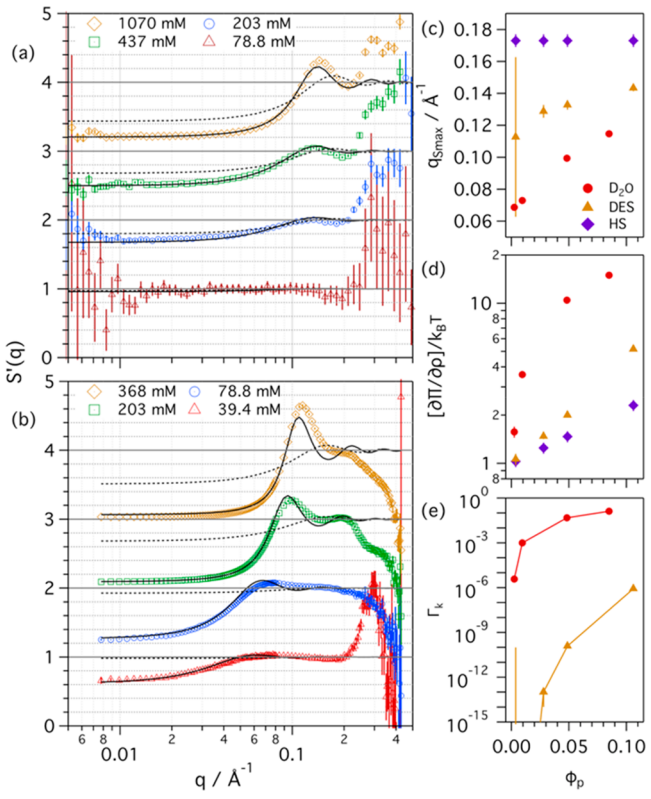

Figure 1. $S(q)'$ data and best fits from different concentrations of h-C_{12}TAC micelles in (a) 1:2 d-ChCl:d-Glyc and (b) D_2O. The concentrations of surfactant are presented in the legend of graph (a) and (b). Data were modeled using the HS model (dotted lines) and RMSA model (solid lines). Data and models were scaled for clarity. Variation of (c) $S'(q)$ first peak position, (d) osmotic compressibility, and (e) Coulomb coupling constant as a function of micelle volume fraction in DES and D_2O, and for HS interactions, as shown in the legend of graph (c). Where not seen, the error bars are within the markers.

Initially, the experimental interparticle scattering was fitted using the HS model, which considers that interparticle interactions are limited to the excluded volume effects (no electrostatics). This approach showed poor agreement between the model and the experimental data, where the calculated intensities and oscillations in the model are far from those in the experimental data. Thus, excluded volume effects from the particle volume are not sufficient to account for the interparticle scattering. Subsequently, the experimental data were fitted using the RMSA model that accounts for electrostatic interactions between colloidal particles.[19,21] As the definition of the structure factor as a function of q implies that $S(q) = 1$ for $q \to \infty$, it should be noted that the lack of agreement for all models for $q > \sim 0.25$ Å^{-1} is attributed to issues with the experimental $S(q)'$ deconvolution process (e.g., background subtraction) and only appears in the high-q data (see Figure S1). Thus, these are assumed to not affect the interpretation of the interparticle interactions from the $S(q)'$ data. The models obtained through this approach successfully describe the experimental data for the surfactant in both DES and D_2O, as seen in Figure 1.

An initial comparison between the interactions observed in DES to those in water and those from the HS theoretical predictions can be made by looking at the position of the first peak in the $S'(q)$ data, q_{Smax} (Figure 1c). This approach is not biased by any modeling assumptions. As the position of the peak in reciprocal space relates to the characteristic distance of correlated particle pairs in real space, lower q-values relate to longer interaction distances. Three initial observations can be made from these results: (1) the position of q_{Smax} changes with concentration for interparticle interactions in DES and water, but only small changes are observed in the position of the HS interaction peak; (2) the peak position goes to higher q-values when increasing particle volume fraction in DES and water; and (3) the q-values in DES are higher than those in water but lower than those from HS predictions. Unlike HS repulsion, the interaction distance between the particles in DES and water must go beyond the characteristic distance of the excluded volume, as observed in the shift of q_{Smax} to lower q-values. Thus, some long-range interactions are present in the systems and the interaction distance appears to be shorter in DES than in D_2O.

From the fitted extrapolated structure factor at zero angle, $S(0)$, the osmotic compressibility for each system can be calculated using the results from the analysis of the scattering data.

$$\frac{1}{S(0)} = \frac{[\partial \Pi/\partial \rho]}{k_B T} \tag{14}$$

And these values can be compared with the osmotic compressibility for hard spheres, which are theoretically predicted using eq 15:[46]

$$\frac{1}{S(0)_{HS}} = \frac{[\partial \Pi/\partial \rho]_{HS}}{k_B T} = \frac{(1 + 2\phi_p)^2}{(1 - \phi_p)^4} \tag{15}$$

Figure 1d shows the calculated $S(0)$ values and a comparison to the HS theoretical predictions. As expected, an increase in particle volume fraction leads to an increase in the osmotic compressibility for all the systems. The results

https://doi.org/10.1021/jacs.1c04781
J. Am. Chem. Soc. 2021, 143, 14158−14168

show that the predictions made by the HS approach are far from the experimental compressibility in DES and water, and this difference increases at larger volume fractions. Also, the trend in the compressibility with ϕ_p in DES is similar to that in water but the absolute values are lower in DES at equivalent particle volume fractions. This again suggests that long-range interactions act upon both systems, but those are weaker in DES.

The observed long-range effects could be attributed to the presence of a strongly correlated shell of solvent components around the micelle (see SI, Figure S3 and Table S4). In this case, the solvent shell around the particles would be invisible to neutrons in terms of particle form factor. However, the presence of this shell would create an excluded volume effect that affects the structure factor contribution to the scattering. To probe this, the experimental structure factor of C_{12}TAC in DES was fitted to an HS model where the effective radius, r_{eff}, and effective volume fraction, $\phi_{p,eff}$, are not constrained to the particle form factor and volume fraction. Thus, these parameters can adopt any arbitrary values that somehow relate to the interparticle interaction. The same analysis was performed for C_{12}TAC in D_2O for comparison. The results show that the fits from this approach are relatively close to the experimental data. This is not surprising as an ersatz excluded volume effect has been previously used to approximate the scattering contribution from long-range interparticle interactions.[29,47] However, different r_{eff} are required to acceptably fit the experimental $S'(q)$ data for different concentrations of surfactant in both DES and aqueous solution. Also, the $\phi_{p,eff}$ are considerably higher than those of the particles, ϕ_p.

Electrostatic interactions between particles can be parametrized through the Coulomb coupling constant, Γ_k. This parameter directly relates to the strength of the interaction potential at the average interparticle distance. Changes in Γ_k for the micelles in DES and water as a function of micelle volume fraction are shown in Figure 1e. It should be noted that this parameter is defined as zero for HS interactions. As with the changes observed in water, the coupling constant increases with micelle volume fraction in DES. The $S'(q)$ effects at low particle volume fraction in DES are very weak, and thus, the uncertainties in the fitted parameters are very large. This value becomes better defined at higher volume fractions but is still several orders of magnitude below the coupling constant for the interactions that occur in water. Therefore, these results confirm that long-range interactions occur in DES, probably electrostatic in nature, and those are weaker in the DES than the repulsion between micelles in water.

Another important effect that governs macroion interactions in colloidal systems is ion condensation and specific ion effects at the particle interface. The experimental scattering data and the apparent structure factor of different counterion-exchanged $C_{12}TA^+$ surfactants in 1:2 d-ChCl:d-Glyc are presented in Figure 2. The fits to the experimental scattering data and results from other surfactant concentrations are included in Figure S2 and Table S2.

As the salt concentration in the DES (ca. 2.5 M) is significantly higher than that of the surfactant native counterion (from 78.8 to 1070 mM), it could be expected that specific ion effects vanish in this environment. However, this is not the case, as micelle morphology is affected by changes in the surfactant counterion despite the dominant concentration of solvent ions. The structural parameters extracted from modeling the form factor show that both r_{eq} and AR vary

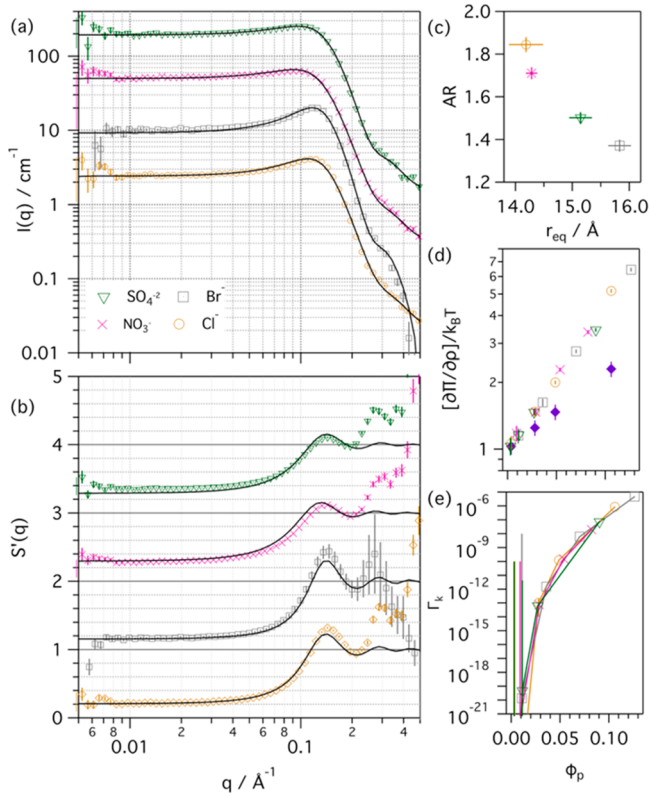

Figure 2. (a) SANS data and (b) $S(q)'$ data of counterion-exchanged 966 mM (average concentration) h-$C_{12}TA^+$ micelles in 1:2 d-ChCl:d-Glyc, as shown in the legend of graph (a). The experimental data were modeled (solid lines) using a uniform ellipsoid form factor and a RMSA structure factor. Data and models were scaled for clarity. Variation of (c) micelle structural parameters r_{eq} and AR, (d) osmotic compressibility, and (e) Coulomb coupling constant as a function of micelle volume faction for each counterion-exchanged surfactant in DES. These results are compared to the theoretical predictions from HS interactions (purple solid markers). Where not seen, the error bars are within the markers.

between the different surfactant counterions, while different concentrations of each surfactant were satisfactorily fitted using the same form factor (see Figure 2c, Figure S2 and Table S2). Also, the fitted micelle volume fractions in DES are considerably lower than the expected values when neglecting monomer content. Considering the total surfactant concentration and the fitted micelle volume fraction, the volume fraction and concentration of surfactant monomers (ϕ_m and $[C_{12}TA^+]_m$, respectively) in solution were calculated as described in the SI. The results are presented in Table 2 for a single surfactant concentration, and a full record of the calculated values for all surfactant concentrations is presented in Table S5. It should be noted that the monomer concentration is only equal to the critical micelle concentration (CMC) at the CMC, and it can evolve in either direction above this threshold concentration in aqueous solution.[48]

The results from the calculations reveal that there is a high concentration of dissolved monomer in solution, and it is counterion dependent. The variation of surfactant solubility follows the trend $[C_{12}TAB]_m < [C_{12}TANO_3]_m < [C_{12}TAC]_m < [C_{12}TA(SO_4)_{1/2}]_m$. Interestingly, the concentration of surfactant monomer increases for all surfactants when the total surfactant concentration is increased (see Table S5),

https://doi.org/10.1021/jacs.1c04781
J. Am. Chem. Soc. 2021, 143, 14158−14168

Table 2. Calculated Monomer Volume Fraction and Concentration of Monomer for Different Surfactant Counterions of h-$C_{12}TA^+$ in 1:2 d-ChCl:d-Glyc: SO_4^{-2}, Br^-, NO_3^-, and Cl^-

Surfactant	$[C_{12}TA^+]$/mM	$\phi_s/\times10^{-2}$	$\phi_p/\times10^{-2}$	$\phi_m/\times10^{-2}$	$[C_{12}TA^+]_m$/mM
h-C_{12}TAC	78.8	2.04	0.35 ± 0.02	1.69 ± 0.02	57.3 ± 0.7
h-C_{12}TAB	79.7	2.43	1.08 ± 0.03	1.34 ± 0.03	45.7 ± 1.0
h-$C_{12}TANO_3$	83.9	2.38	0.90 ± 0.02	1.48 ± 0.02	50.3 ± 0.7
h-$C_{12}TA(SO_4)_{1/2}$	85.8	2.32	0.29 ± 0.04	2.01 ± 0.04	69.1 ± 1.4

proving that the surfactant monomer concentration is not constant above the CMC.

The long-range interactions of counterion-exchanged surfactant micelles were also probed using these data (Figure 2b). For all these surfactants in DES, it is seen that the osmotic compressibility is higher than those values from the HS theoretical predictions and these excess interactions are hypothesized again to be of electrostatic origin. When comparing the osmotic compressibility for the different surfactants (Figure 2d), the results follow a similar trend and only small differences are observed. Also, the results for the Coulomb coupling constant follow the same trends and only subtle differences between the various counterion-exchanged surfactants are observed. To directly compare the strength of the electrostatic interactions, the experimental coupling constants were modeled using a simple empirical approach and the coupling constants of the different systems were calculated for a theoretical volume fraction of 10% using those models (see SI, Figure S4, Table S6). Among the counterions investigated here, it is observed that the coupling constant for ϕ_p = 0.1 of h-C_{12}TAB and h-$C_{12}TANO_3$ in 1:2 d-ChCl:d-Glyc are 31% (±5%) and 56% (±8%) lower than that for h-C_{12}TAC, respectively. On the contrary, the coupling constant for h-$C_{12}TA(SO_4)_{1/2}$ at the same volume fraction is 13% (±4%) higher than that for h-C_{12}TAC. These observations confirm that the strength of the intermicellar interactions depends on the surfactant counterion, where it follows the trend, from weaker to stronger, $NO_3^- < Br^- < Cl^- < O_4^{-2}$. As such, the specific ion effects also modulate long-range interparticle interactions in the DES.

Due to the ionic nature of the DES, it is hypothesized that the resulting ion-pair interactions rely on a balance between the interactions of the surfactant counterion with either the micelle or the ionic species in the bulk solvent. To prove this, we have investigated the self-assembly of d-C_{12}TAB in 1:2 h-ChBr:h-Glyc and compared that to the behavior of h-C_{12}TAC in 1:2 d-ChCl:d-Glyc. This study provides an insight into the role of the main ions involved in the condensation of counterions at the interface of the cationic micelles. The experimental scattering data and models for d-C_{12}TAB in 1:2 h-ChBr:h-Glyc are presented in Figure 3. The results from the analysis are presented in Table S3.

It is important to note that, due to the lack of data on the physicochemical properties of the bromide-based DES, those values were approximated as those of the chloride-based DES for data analysis purposes. When comparing the results from the data analysis, small differences in micelle structure were found between the two systems (see Tables S1 and S3). The calculated osmotic compressibility of d-C_{12}TAB micelles in 1:2 h-ChBr:h-Glyc increases with increasing micelle volume fraction (see Figure 3c), as observed for the system in the chloride-based DES. However, these values are lower than those for h-C_{12}TAC micelles in 1:2 d-ChCl:d-Glyc and again higher than those from HS predictions. When comparing the

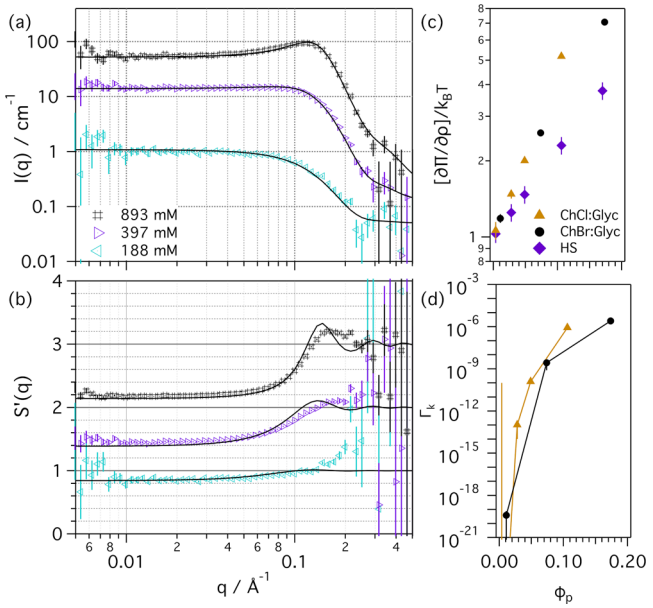

Figure 3. (a) SANS data and (b) $S(q)'$ data from different concentrations of d-C_{12}TAB micelles in 1:2 h-ChBr:h-Glyc, as shown in the legend of graph (a). The experimental data were modeled (solid lines) using a uniform ellipsoid form factor and an RMSA structure factor. Data and models were scaled for clarity. Variation of (c) osmotic compressibility and (d) Coulomb coupling constant as a function of micelle volume faction for d-C_{12}TAB micelles in 1:2 h-ChBr:h-Glyc and h-C_{12}TAC micelles in 1:2 d-ChCl:d-Glyc, and for HS interactions, as shown in the legend of graph (c). Where not seen, the error bars are within the markers.

values from the Coulomb coupling constant (see Figure 3d), it is seen that the strength of the intermicellar interactions in 1:2 h-ChBr:h-Glyc is slightly lower than that in 1:2 d-ChCl:d-Glyc, in line with the osmotic compressibility results. Therefore, electrostatic interactions between micelles are weaker in the bromide-based DES than in the chloride analogue.

DISCUSSION

Long-Range Electrostatic Colloidal Interactions. The interactions attributed to HS packing, commonly used to fit the scattering from uncharged or screened micelles,[37] are not appropriate to describe the behavior of h-C_{12}TAC micelles in either d-DES or D_2O, and an excess interaction seems to act upon the system. When attempting to fit the intermicellar structure factor using the RMSA model, which describes long-range electrostatic interactions between colloidal particles, good agreement between data and models was found. This agreement suggests that the excess interparticle interaction in DES may be attributed to the Coulombic repulsion between the macroions in solution, as it occurs in water.[49] The main difference observed in the interactions between h-C_{12}TAC micelles in d-DES or D_2O is that those are weaker in the case of the DES, suggesting that the electrostatic interactions are

https://doi.org/10.1021/jacs.1c04781
J. Am. Chem. Soc. 2021, 143, 14158−14168

partially screened in DES compared to those in water. Another model that could be considered to describe the long-range effects in DES is that resulting from the excluded volume between strongly correlated solvent shells around the micelles. From the analysis of the experimental structure factor using an effective excluded volume to account for this shell (see SI, Figure S3, Table S4), it is observed that the effective radius varies with surfactant concentration for the C_{12}TAC micelles in DES and aqueous solution. As the solvation of the particle is not expected to change with the C_{12}TAC concentration, the r_{eff}, i.e. the "hard" solvation shell around the particle, should remain constant if the long-range interactions were solely attributed to the overlap between these shells. As this value changes with surfactant concentration, the long-range interactions cannot be attributed to the exclusion between correlated solvent shells around the micelle.

One of the main contributions to the differences in the strength of the interaction between these two solvents must arise from differences in the permittivity and ionic strength of the continuum, parametrized here as the Debye length. In order to rationalize the difference in the strength of the interaction, we first consider a thought experiment: Assuming the same arbitrary ionic strength for the two solvents (e.g., 20 mM), the differences in the calculated Debye lengths will only depend on the solvent permittivity (ε_{DES} = 22.8 and ε_{water} = 77.9). As such, the Debye lengths in this hypothetical case are ∼12 Å and ∼22 Å for DES and water, respectively, which is a ca. 45% difference in the Debye length between these two electrolytes. When estimating the Coulomb coupling constant for an arbitrary particle charge (e.g., 30), the difference in the values between these two solvents becomes ca. 450%. However, the difference in the Coulomb coupling constant from the analysis of the scattering data is around 6 orders of magnitude larger in water than in DES. As the permittivity of the solvents does not suffice to account for the difference in the coupling constant, there must also be a significant contribution from the ionic strength of the continuum.

From theoretical calculations, it is seen that the coupling constant rapidly decays when increasing the ionic strength of the solvent as interactions at the average interparticle distance become weaker (see SI, Table S7, Figure S5). However, the coupling constant values in DES are still above zero, showing that excluded volume effects without long-range effects are not sufficient to account for the interparticle interactions. Therefore, the apparent ionic strength of the DES must be much higher than that of D_2O, as could be expected. Due to the mathematical correlation between the solvent ionic strength and particle charge in the calculation of the surface potential and Coulomb coupling constant (eqs 5, 6, and 7), these parameters could not be accurately calculated. To shed some light on how these vary for the fitted coupling constant, a sensitivity analysis was performed (see SI, Table S8). From this analysis, it is observed that the effective ionic strength of the solvent falls between ca. 340 and 540 mM for a realistic range of macroion charges (assuming counterion dissociations between 20% and 80%). This confirms that the effective ionic strength of the DES is significantly lower than the theoretical ionic strength of this solvent (ca. 2.5 M, as calculated from the complete dissociation of choline chloride), which in turn would lead to negligible Debye lengths (ca. 1.5 Å) and the absence of long-range electrostatic interactions. Consequently, the Debye length of the DES appears to be considerably larger than the theoretical Debye length for this solvent, as some partially screened electrostatic interactions between particles prevail in DES. One of the remaining challenges to quantify the effects of electrostatic interactions and counterion condensation (e.g., particle surface charge) is to accurately characterize the ionic character of the DES (e.g., Debye length). This will provide a better understanding of the fundamental effects presented here and will enable direct comparison to other highly ionic systems.

Considering these results, parallels can be drawn with the behavior of concentrated electrolytes and ionic liquids. As it has recently been shown for long-range electrostatics in systems with a high ion concentration, the apparent screening length is much larger than that theoretically predicted by the Debye−Hückel theory.[8,9,50] This effect has been associated with the strong ion−ion correlations within the bulk phase in concentrated ionic environments. As such, the bulk liquid is mainly constituted by strongly correlated ions that do not effectively contribute to the ionic strength of the solvent, while a relatively small number of thermally excited ions can act as charge carriers.[51] Thus, the resulting screening effect is much weaker than that for noncorrelated ions and the system behaves as a relatively dilute electrolyte. We hypothesized here that an analogous effect is observed in DES: ion-pair correlations within the bulk reduce the apparent ionic strength of the solvent and are the mechanistic origin of the long-range electrostatic interactions in DES. In the case of DES, it could be expected that the system behaves in a similar way to highly concentrated ionic solutions in neutral solvents.[52] The neutral moiety of the DES would contribute to the partial disruption of ion-pair correlations and allow a certain population of free ions.

The ion−ion correlation in DES has also been evidenced by other investigations. For example, the ion conductivity decreased in neat DES compared to hydrated DES, in stark contrast to dilute electrolytes that increase conductivity with increasing salt content.[53] As the salt concentration in the DES components increases with decreasing hydration level, ion mobility is hindered by molecular interactions between the solvent constituents, resulting in a strong ion−ion correlation and low conductivity. Also, it has been shown that the charged surface of colloidal particles induces fluctuations in the structure of the solvent and the formation of multilayer perturbations, possibly attributed to electrostatic interactions that extend beyond the nanometer scale.[54,55] Similarly, the nanostructure of the solvent was found to be affected up to a few nanometers at the platinum−DES interface with applied potential.[56] Molecular dynamic simulations showed that charge spreading occurs through the DES network, resulting in an effective charge density lower than that of the compounds in an ideal gas phase.[57] Thus, the hypothesis of the prevalence of long-range electrostatic effects in DES as the result of strong ion−ion correlation in the continuum is further supported by previous studies using a variety of methods.

Specific Ion Effects. The condensation of ions at the micelle interface, either the native surfactant counterion or from added salts, is a well-known effect in aqueous solution, where this modulates electrostatic interactions, affects monomer solubility, and results in changes in micelle morphology.[58−61] Here, we show that different surfactant counterions lead to variations in micelle structure in the DES, as the radius and aspect ratio of the micelle changes. Also, the monomer solubility changes with varying the counterion and volume fraction of surfactant. These effects have previously

https://doi.org/10.1021/jacs.1c04781
J. Am. Chem. Soc. 2021, 143, 14158−14168

been reported for anionic surfactant micelles in DES, where the substitution of the counterion in dodecylsulfate surfactant solutions resulted in changes in micelle morphology and CMC.[62] Similarly, other specific charge interactions with hydrotropes and solvent ions have been shown to affect the morphology of micelles in DES.[47,63−65]

The relatively high concentration of surfactant monomers could relate to the weaker solvophobic effect in DES compared to that in water.[66] For instance, the CMC of C_{12}TAB in 1:2 choline chloride:glycerol (CMC = 22 mM) has been shown to be higher than those in aqueous solution (CMC = 15 mM), but significantly lower than that in ethylammonium nitrate (190 mM).[29,67,68] The weaker solvophobic effect also results in a higher monomer concentration in the micellar phase, and the solubilized surfactant monomers in 1:2 choline chloride:glycerol could deviate the solvent from its native composition and structure. Previous investigations have shown that an imbalance in the eutectic composition affects the molecular behavior of DES.[69] However, the presence of a neutrally charged graphite interface, which could cause similar effects in the solvent structure to those induced by the hydrophobic surfactant tails, only prompts subtle short-range changes in the molecular ordering of 1:2 choline chloride:glycerol.[70] At the surfactant concentrations investigated here, these local changes are not expected to alter the bulk behavior of the DES, as correlations between the solvent components are relatively resilient.[11,71] Also, the trends observed in intermicellar interactions and the unchanged micelle morphology in the concentration range investigated here suggest that no significant changes in the behavior of the solvent occur when increasing the surfactant content. However, further investigations are required to probe the presence of specific surfactant−DES interactions at the molecular level.

Specific ion effects have also been reported for the micellization of surfactants in aqueous electrolytes and ionic liquids. Small-angle neutron scattering was used to demonstrate that the adsorption of surfactant counterions controls the micellization in protic ionic liquids, affecting the structure of the globular micelles due to specific counterion condensation.[72] Interestingly, whereas $C_{12}TA^+$ micelles in water increase in aggregation number with addition of salt which results in the formation of elongated micelles,[73] these remain globular in DES and ionic liquids despite the high ionic strength of the solvent.[72] Also, the solubility of surfactant monomer has been shown to vary in ionic liquids depending on the surfactant counterion.[72] The observed variation of surfactant monomer concentration above the CMC is an effect that has previously been reported for C_{12}TAB in aqueous solution, where the monomer concentration gradually decreases above the CMC with increasing surfactant concentrations.[48,74] However, it is observed that the content of solubilized monomer above the CMC follows the opposite trend in DES. The mechanistic origin of this stark difference is however unknown, and there must be a deeper meaning related to the surfactant activity and monomer−micelle equilibrium.

The effect of counterion exchange is also shown to modulate electrostatic interactions between particles in DES, as previously shown for aqueous solutions of micelles.[61,75] It is hypothesized that certain ions are more prone to condense at the micelle interface and screen interparticle interactions to a larger extent in DES, following a similar mechanism to that in water. The condensation of counterions will potentially result in a change in the surface potential of the micelle, which is the main source for the differences in the coupling constants between the different counterion-exchanged surfactant systems, as the ionic strength of the continuum will remain relatively unchanged. Interestingly, the strength of the interaction follows the same order as it does in water (from weaker to stronger, $NO_3^- < Br^- < Cl^- < SO_4^{-2}$).[75] These specific condensation effects have also been observed for colloidal particles in DES, where exogenous Ag^+ ions were found to preferentially populate regions around SiO_2 particles, demonstrating that specific ion−ion interactions occur to the detriment of choline−particle interactions.[54]

These specific ion effects are attributed to the energetic balance between the ion in a solvated state and that in a condensed state, ultimately leading to counterion condensation. This balance differs depending on the character of the ion and have traditionally been described by the Hofmeister or lyotropic series in aqueous solutions, ionic liquids, and other nonaqueous solvents.[75−77] For instance, it is expected that a bromide counterion will interact more strongly with a cationic micelle than chloride, which in turn will remain more solvated and result in a more pronounced electrostatic effect. This is a similar behavior to that observed in the case of the cationic micelles investigated here, where the coupling constants for the bromide and nitrate counterions are lower than those for the chloride and sulfate counterions. It is expected that the trends in terms of counterion solubility follow the opposite order: $NO_3^- < Br^- < Cl^- < SO_4^{-2}$. Therefore, the Hofmeister series can describe specific ion effects in DES.

It has recently been shown that electronic perturbations as induced by ion pairs and ion−solvent interactions are the underlying phenomena that control ion solvation and condensation effects in aqueous and nonaqueous molecular solvents.[78] These findings could also be used to describe the specific ion effects in DES. Unlike in aqueous solution where the ion effects can simply be rationalized in terms of the interaction between a pair of ionic species,[75] these effects in DES are far more complex due to the ionic character of the solvent. As the ion-pair interaction relies on a balance between the counterion−headgroup interactions (i.e., ion condensation free energy) and the counterion−solvent interactions (i.e., ion solvation free energy), the resulting counterion condensation will be defined by the interplay between these two ionic perturbations. This has been shown for the self-assembly of surfactants in ternary DES, where the solubility of the counterion modulates micelle morphology.[65] There, the reduction of the solubility was shifting the energetic balance toward the condensed state at the micelle interface. This was investigated here by comparing the long-range interactions in the counterion-exchanged solvents. As the surfactant counterion is the same as the solvent anion (Br^- in 1:2 h-ChBr:h-Glyc, Cl^- in 1:2 d-ChCl:d-Glyc), no specific ion−solvent effects are expected for these systems. As such, the differences in the electrostatics are mainly attributed to the dissociation of surfactant counterions in each solvent and the permittivity of those (here assumed to be the same for analysis purposes). The results showed that stronger electrostatic interactions appear in the case of the h-C_{12}TAC solution in 1:2 d-ChCl:d-Glyc in comparison to the d-C_{12}TAB solution in 1:2 h-ChBr:h-Glyc. This shows that the association of Cl^- counterions with the cationic micelles is weaker than that of Br^-, thus confirming the specificity of the counterion condensation.

https://doi.org/10.1021/jacs.1c04781
J. Am. Chem. Soc. 2021, 143, 14158−14168

CONCLUSIONS

Deep eutectic solvents are promising sustainable alternatives to traditional solvents in a vast array of technological products and processes. From mimicking biological environments in the absence of water for biomolecule preservation to the development of cheap and green electrolytes, understanding the fundamental phenomena that govern electrostatic interactions in DES opens new avenues for research. Here, we presented the first investigation of electrostatic interactions in DES. Small-angle neutron scattering was used to probe particle structure and particle−particle correlation in micellar systems dispersed in 1:2 choline chloride:glycerol and 1:2 choline bromide:glycerol.

The results show that long-range interactions prevail in DES and are electrostatic in origin. These interactions are weaker than those for the analogous system in aqueous solution, and this was attributed to the higher ionic strength of the DES. However, this effective ionic strength seems to be much lower than the actual ion concentration in the DES (*ca.* 2.5 M), which would lead to negligible long-range electrostatics. The mechanistic origin of these electrostatic interactions is hypothesized to arise from the strong ion-pair correlation in DES, where strong short-range correlations between ions within the solvent reduce the apparent ionic strength in DES. This parallels recent theories on the behavior of charge interactions in ionic liquids and concentrated electrolytes.

Also, specific ion effects, which play a key role in colloidal stability and protein behavior, are demonstrated to modulate micelle morphology, surfactant solubility, and long-range electrostatic interactions in DES. These effects were attributed to the counterion condensation at the micelle interface, and the Hofmeister series can be used to describe the observed trends. These interactions are classically described as a single ion pair in water, where the free energy of solvation/condensation controls the extent of the adsorption. However, the mechanism seems to be more complex in DES, where electrostatic correlations within the solvent potentially affect the interactions of the counterion with the surfactant.

As such, DES join the group of solvents with high ion concentrations (i.e., concentrated electrolytes and ionic liquids) that challenge the traditional understanding of electrostatic interactions. Therefore, the investigations presented here will have diverse implications in fundamental and applied research. For instance, a better understanding of the electrostatic and ion-specific effects in DES will influence the development of new colloidal systems, the design of novel environments for the stabilization and function of biomolecules, and the preparation of sustainable electrolytes using DES. Also, these results contribute to the development of a benchmark theory that describes electrostatic interactions in concentrated ionic environments.

ASSOCIATED CONTENT

Supporting Information

The Supporting Information is available free of charge at https://pubs.acs.org/doi/10.1021/jacs.1c04781.

A detailed description of the preparation of the counterion exchanged surfactants, a record of the SANS data modeling, the results from the calculation of the monomer concentration in DES, and the modeling approach of the Coulomb coupling constant. Data supporting this article has been made available at DOI: 10.5286/ISIS.E.RB1620126. (PDF)

AUTHOR INFORMATION

Corresponding Author

Adrian Sanchez-Fernandez − *Food Technology, Engineering and Nutrition, Lund University, 221 00 Lund, Sweden;* orcid.org/0000-0002-0241-1191; Email: adrian.sanchez-fernandez@food.lth.se

Authors

Andrew J. Jackson − *European Spallation Source, 221 00 Lund, Sweden; Department of Physical Chemistry, Lund University, Lund, SE 221 00, Sweden;* orcid.org/0000-0002-6296-0336

Sylvain F. Prévost − *Institut Laue-Langevin, 38000 Grenoble, France;* orcid.org/0000-0002-6008-1987

James J. Doutch − *ISIS Neutron and Muon Source, Science and Technology Facilities Council, Didcot OX11 0QX, U.K.;* orcid.org/0000-0003-0747-8368

Karen J. Edler − *Department of Chemistry, University of Bath, Bath BA2 7AY, U.K.;* orcid.org/0000-0001-5822-0127

Complete contact information is available at: https://pubs.acs.org/10.1021/jacs.1c04781

Notes

The authors declare no competing financial interest.

ACKNOWLEDGMENTS

The authors would like to thank the European Spallation Source and the University of Bath Alumni Fund for funding A.S.-F. The research activities were also supported by Vinnova − Swedish Governmental Agency for Innovation Systems within the NextBioForm Competence Centre, and the Crafoord Foundation (Grant 20190750). The authors thank ISIS Pulsed Neutron and Muon Source (RB1620126) and Institute Laue-Langevin (9-13-820) for the awarded beamtime. We would like to thank Dr. Wojciech Potrzebowski (European Spallation Source) for the fruitful discussions on the implementation of structure factor models in SasView. This work benefited from the use of the SasView application, originally developed under NSF award DMR-0520547. SasView contains code developed with funding from the European Union's Horizon 2020 research and innovation programme under the SINE2020 project, Grant Agreement No. 654000.

REFERENCES

(1) Urban, A.; Seo, D.-H.; Ceder, G. Computational understanding of Li-ion batteries. *npj Computational Materials* **2016**, *2* (1), 16002.
(2) Zhou, H. X.; Pang, X. Electrostatic Interactions in Protein Structure, Folding, Binding, and Condensation. *Chem. Rev.* **2018**, *118* (4), 1691−1741.
(3) Eisenberg, B. Interacting ions in biophysics: real is not ideal. *Biophys. J.* **2013**, *104* (9), 1849−66.
(4) Debye, P.; Hückel, E. The theory of electrolytes: I. lowering of freezing point and related phenomena. *Z. Phys.* **1923**, *24*, 185−206.
(5) Derjaguin, B. V.; Churaev, N. V.; Muller, V. M. The Derjaguin−Landau−Verwey−Overbeek (DLVO) Theory of Stability of Lyophobic Colloids. In *Surface Forces*, Derjaguin, B. V.; Churaev, N. V.; Muller, V. M., Eds.; Springer US: Boston, MA, 1987; pp 293−310.
(6) Zhang, Y.; Cremer, P. S. Interactions between macromolecules and ions: The Hofmeister series. *Curr. Opin. Chem. Biol.* **2006**, *10* (6), 658−63.

(7) Collins, K. D. Why continuum electrostatics theories cannot explain biological structure, polyelectrolytes or ionic strength effects in ion-protein interactions. *Biophys. Chem.* **2012**, *167*, 43−59.
(8) Lee, A. A.; Perez-Martinez, C. S.; Smith, A. M.; Perkin, S. Scaling Analysis of the Screening Length in Concentrated Electrolytes. *Phys. Rev. Lett.* **2017**, *119* (2), 026002.
(9) Gebbie, M. A.; Smith, A. M.; Dobbs, H. A.; Lee, A. A.; Warr, G. G.; Banquy, X.; Valtiner, M.; Rutland, M. W.; Israelachvili, J. N.; Perkin, S.; Atkin, R. Long range electrostatic forces in ionic liquids. *Chem. Commun. (Cambridge, U. K.)* **2017**, *53* (7), 1214−1224.
(10) Hammond, O. S.; Bowron, D. T.; Edler, K. J. Liquid structure of the choline chloride-urea deep eutectic solvent (reline) from neutron diffraction and atomistic modelling. *Green Chem.* **2016**, *18* (9), 2736−2744.
(11) Hammond, O. S.; Bowron, D. T.; Jackson, A. J.; Arnold, T.; Sanchez-Fernandez, A.; Tsapatsaris, N.; Garcia Sakai, V.; Edler, K. J. Resilience of Malic Acid Natural Deep Eutectic Solvent Nanostructure to Solidification and Hydration. *J. Phys. Chem. B* **2017**, *121* (31), 7473−7483.
(12) Abbott, A. P.; Harris, R. C.; Ryder, K. S.; D'Agostino, C.; Gladden, L. F.; Mantle, M. D. Glycerol eutectics as sustainable solvent systems. *Green Chem.* **2011**, *13* (1), 82−90.
(13) Sanchez-Fernandez, A.; Jackson, A. J., Proteins in deep eutectic solvents: Structure, dynamics and interactions with the solvent. In *Eutectic Solvents and Stress in Plants*, in press; Verpoorte, R., Ed.; Elsevier: 2020.
(14) Ballantyne, A. D.; Barker, R.; Dalgliesh, R. M.; Ferreira, V. C.; Hillman, A. R.; Palin, E. J. R.; Sapstead, R.; Smith, E. L.; Steinke, N.-J.; Ryder, K. S. Electrochemical deposition of silver and copper from a deep eutectic solvent studied using time-resolved neutron reflectivity. *J. Electroanal. Chem.* **2018**, *819*, 511−523.
(15) Hammond, O. S.; Edler, K. J.; Bowron, D. T.; Torrente-Murciano, L. Deep eutectic-solvothermal synthesis of nanostructured ceria. *Nat. Commun.* **2017**, *8*, 14150.
(16) Jiang, P.; Chen, L.; Shao, H.; Huang, S.; Wang, Q.; Su, Y.; Yan, X.; Liang, X.; Zhang, J.; Feng, J.; Liu, Z. Methylsulfonylmethane-Based Deep Eutectic Solvent as a New Type of Green Electrolyte for a High-Energy-Density Aqueous Lithium-Ion Battery. *ACS Energy Letters* **2019**, *4* (6), 1419−1426.
(17) Gertrudes, A.; Craveiro, R.; Eltayari, Z.; Reis, R. L.; Paiva, A.; Duarte, A. R. C. How Do Animals Survive Extreme Temperature Amplitudes? The Role of Natural Deep Eutectic Solvents. *ACS Sustainable Chem. Eng.* **2017**, *5* (11), 9542−9553.
(18) Percus, J. K.; Yevick, G. J. Analysis of Classical Statistical Mechanics by Means of Collective Coordinates. *Phys. Rev.* **1958**, *110* (1), 1−13.
(19) Hansen, J.-P.; Hayter, J. B. A rescaled MSA structure factor for dilute charged colloidal dispersions. *Mol. Phys.* **1982**, *46* (3), 651−656.
(20) Hayter, J. B.; Penfold, J. An analytic structure factor for macroion solutions. *Mol. Phys.* **1981**, *42* (1), 109−118.
(21) Qiu, D.; Dreiss, C. A.; Cosgrove, T.; Howe, A. M. Small-angle neutron scattering study of concentrated colloidal dispersions: the interparticle interactions between sterically stabilized particles. *Langmuir* **2005**, *21* (22), 9964−9.
(22) Reus, V.; Belloni, L.; Zemb, T.; Lutterbach, N.; Versmold, H. Equation of State and Structure of Electrostatic Colloidal Crystals: Osmotic Pressure and Scattering Study. *J. Phys. II* **1997**, *7* (4), 603−626.
(23) Lu, J. R.; Marrocco, A.; Su, T. J.; Thomas, R. K.; Penfold, J. Adsorption of Dodecyl Sulfate Surfactants with Monovalent Metal Counterions at the Air-Water Interface Studied by Neutron Reflection and Surface Tension. *J. Colloid Interface Sci.* **1993**, *158* (2), 303−316.
(24) Heenan, R. K.; Rogers, S. E.; Turner, D.; Terry, A. E.; Treadgold, J.; King, S. M. Small Angle Neutron Scattering Using Sans2d. *Neutron News* **2011**, *22* (2), 19−21.
(25) Lieutenant, K.; Lindner, P.; Gahler, R. A new design for the standard pinhole small-angle neutron scattering instrument D11. *J. Appl. Crystallogr.* **2007**, *40* (6), 1056−1063.
(26) Arnold, O.; Bilheux, J. C.; Borreguero, J. M.; Buts, A.; Campbell, S. I.; Chapon, L.; Doucet, M.; Draper, N.; Ferraz Leal, R.; Gigg, M. A.; Lynch, V. E.; Markvardsen, A.; Mikkelson, D. J.; Mikkelson, R. L.; Miller, R.; Palmen, K.; Parker, P.; Passos, G.; Perring, T. G.; Peterson, P. F.; Ren, S.; Reuter, M. A.; Savici, A. T.; Taylor, J. W.; Taylor, R. J.; Tolchenov, R.; Zhou, W.; Zikovsky, J. Mantid—Data analysis and visualization package for neutron scattering and μ SR experiments. *Nucl. Instrum. Methods Phys. Res., Sect. A* **2014**, *764*, 156−166.
(27) Richard, D.; Ferrand, M.; Kearley, G. J. Analysis and visualisation of neutron-scattering data. *J. Neutron Res.* **1996**, *4* (1), 33−39.
(28) Barker, J. G.; Pedersen, J. S. Instrumental Smearing Effects in Radially Symmetric Small-Angle Neutron Scattering by Numerical and Analytical Methods. *J. Appl. Crystallogr.* **1995**, *28* (2), 105−114.
(29) Sanchez-Fernandez, A.; Arnold, T.; Jackson, A. J.; Fussell, S. L.; Heenan, R. K.; Campbell, R. A.; Edler, K. J. Micellization of alkyltrimethylammonium bromide surfactants in choline chloride:glycerol deep eutectic solvent. *Phys. Chem. Chem. Phys.* **2016**, *18* (48), 33240−33249.
(30) Pedersen, J. S. Analysis of small-angle scattering data from colloids and polymer solutions: modeling and least-squares fitting. *Adv. Colloid Interface Sci.* **1997**, *70*, 171−210.
(31) Marcus, Y. *Ion properties*; CRC Press: 1997.
(32) Tanford, C. Micelle shape and size. *J. Phys. Chem.* **1972**, *76* (21), 3020−3024.
(33) Mukerjee, P. Size distribution of small and large micelles. Multiple equilibrium analysis. *J. Phys. Chem.* **1972**, *76* (4), 565−570.
(34) Kotlarchyk, M.; Chen, S. H. Analysis of small angle neutron scattering spectra from polydisperse interacting colloids. *J. Chem. Phys.* **1983**, *79* (5), 2461−2469.
(35) Ornstein, L. S.; Zernike, F. Accidental deviations of density and opalescence at the critical point of a single substance. *Proc. Acad. Sci. Amsterdam* **1914**, *17*, 15.
(36) Pedersen, J. S. Determination of size distribution from small-angle scattering data for systems with effective hard-sphere interactions. *J. Appl. Crystallogr.* **1994**, *27* (4), 595−608.
(37) van Osch, D. J. G. P.; Dietz, C. H. J. T.; Warrag, S. E. E.; Kroon, M. C. The Curious Case of Hydrophobic Deep Eutectic Solvents: A Story on the Discovery, Design, and Applications. *ACS Sustainable Chem. Eng.* **2020**, *8* (29), 10591−10612.
(38) Greene, D. G.; Ferraro, D. V.; Lenhoff, A. M.; Wagner, N. J. A critical examination of the decoupling approximation for small-angle scattering from hard ellipsoids of revolution. *J. Appl. Crystallogr.* **2016**, *49* (5), 1734−1739.
(39) Pedersen, J. Determination of size distribution from small-angle scattering data for systems with effective hard-sphere interactions. *J. Appl. Crystallogr.* **1994**, *27* (4), 595−608.
(40) Doucet, M.; Cho, J. H.; Alina, G.; Attala, Z.; Bakker, J.; Bouwman, W.; Butler, P.; Campbell, K.; Cooper-Benun, T.; Durniak, C.; Forster, L.; Gonzales, M.; Heenan, R.; Jackson, A.; King, S.; Kienzle, P.; Krzywon, J.; Nielsen, T.; O'Driscoll, L.; Potrzebowski, W.; Prescott, S.; Ferraz Leal, R.; Rozycko, P.; Snow, T.; Washington, A. SasView version 5.0.3. https://zenodo.org/record/3930098 (accessed 2020-08-24).
(41) Li, Q.; Wang, J.; Lei, N.; Yan, M.; Chen, X.; Yue, X. Phase behaviours of a cationic surfactant in deep eutectic solvents: from micelles to lyotropic liquid crystals. *Phys. Chem. Chem. Phys.* **2018**, *20* (17), 12175−12181.
(42) Sanchez-Fernandez, A. Self-assembly in deep eutectic solvents. Thesis (Ph.D.), University of Bath, 2018.
(43) Hayter, J. B.; Penfold, J. Determination of micelle structure and charge by neutron small-angle scattering. *Colloid Polym. Sci.* **1983**, *261* (12), 1022−1030.
(44) Agieienko, V.; Buchner, R. Dielectric relaxation of deep eutectic solvent + water mixtures: structural implications and application to microwave heating. *Phys. Chem. Chem. Phys.* **2020**, *22* (36), 20466−20476.

(45) Malmberg, C. G. Dielectric constant of deuterium oxide. *Journal of Research of the National Bureau of Standards* **1958**, *60* (6), 609−612.
(46) Van Helden, A. K.; Vrij, A. Static light scattering of concentrated silica dispersions in apolar solvents. *J. Colloid Interface Sci.* **1980**, *78* (2), 312−329.
(47) Sanchez-Fernandez, A.; Hammond, O. S.; Jackson, A. J.; Arnold, T.; Doutch, J.; Edler, K. J. Surfactant-Solvent Interaction Effects on the Micellization of Cationic Surfactants in a Carboxylic Acid-Based Deep Eutectic Solvent. *Langmuir* **2017**, *33* (50), 14304−14314.
(48) Danov, K. D.; Kralchevsky, P. A.; Ananthapadmanabhan, K. P. Micelle-monomer equilibria in solutions of ionic surfactants and in ionic-nonionic mixtures: a generalized phase separation model. *Adv. Colloid Interface Sci.* **2014**, *206*, 17−45.
(49) Hayter, J. B.; Penfold, J. Self-consistent structural and dynamic study of concentrated micelle solutions. *J. Chem. Soc., Faraday Trans. 1* **1981**, *77* (8), 1851.
(50) Smith, A. M.; Lee, A. A.; Perkin, S. The Electrostatic Screening Length in Concentrated Electrolytes Increases with Concentration. *J. Phys. Chem. Lett.* **2016**, *7* (12), 2157−63.
(51) Kjellander, R. Decay behavior of screened electrostatic surface forces in ionic liquids: the vital role of non-local electrostatics. *Phys. Chem. Chem. Phys.* **2016**, *18* (28), 18985−9000.
(52) Bozym, D. J.; Uralcan, B.; Limmer, D. T.; Pope, M. A.; Szamreta, N. J.; Debenedetti, P. G.; Aksay, I. A. Anomalous Capacitance Maximum of the Glassy Carbon-Ionic Liquid Interface through Dilution with Organic Solvents. *J. Phys. Chem. Lett.* **2015**, *6* (13), 2644−8.
(53) Shah, D.; Mjalli, F. S. Effect of water on the thermo-physical properties of Reline: An experimental and molecular simulation based approach. *Phys. Chem. Chem. Phys.* **2014**, *16* (43), 23900−7.
(54) Hammons, J. A.; Zhang, F.; Ilavsky, J. Extended hierarchical solvent perturbations from curved surfaces of mesoporous silica particles in a deep eutectic solvent. *J. Colloid Interface Sci.* **2018**, *520*, 81−90.
(55) Hammons, J. A.; Ustarroz, J.; Muselle, T.; Torriero, A. A. J.; Terryn, H.; Suthar, K.; Ilavsky, J. Supported Silver Nanoparticle and Near-Interface Solution Dynamics in a Deep Eutectic Solvent. *J. Phys. Chem. C* **2016**, *120* (3), 1534−1545.
(56) Hammond, O. S.; Li, H.; Westermann, C.; Al-Murshedi, A. Y. M.; Endres, F.; Abbott, A. P.; Warr, G. G.; Edler, K. J.; Atkin, R. Nanostructure of the deep eutectic solvent/platinum electrode interface as a function of potential and water content. *Nanoscale Horiz* **2019**, *4* (1), 158−168.
(57) Zahn, S.; Kirchner, B.; Mollenhauer, D. Charge Spreading in Deep Eutectic Solvents. *ChemPhysChem* **2016**, *17* (21), 3354−3358.
(58) Bergström, M.; Skov Pedersen, J. Structure of pure SDS and DTAB micelles in brine determined by small-angle neutron scattering (SANS). *Phys. Chem. Chem. Phys.* **1999**, *1* (18), 4437−4446.
(59) Liu, Y. C.; Chen, S. H.; Itri, R. Ion correlations and counter-ion condensation in ionic micellar solutions. *J. Phys.: Condens. Matter* **1996**, *8* (25A), A169−A187.
(60) Kuperkar, K.; Abezgauz, L.; Prasad, K.; Bahadur, P. Formation and Growth of Micelles in Dilute Aqueous CTAB Solutions in the Presence of NaNO3 and NaClO3. *J. Surfactants Deterg.* **2010**, *13* (3), 293−303.
(61) Aswal, V. K.; Goyal, P. S. Role of different counterions and size of micelle in concentration dependence micellar structure of ionic surfactants. *Chem. Phys. Lett.* **2003**, *368* (1−2), 59−65.
(62) Sanchez-Fernandez, A.; Hammond, O. S.; Edler, K. J.; Arnold, T.; Doutch, J.; Dalgliesh, R. M.; Li, P.; Ma, K.; Jackson, A. J. Counterion binding alters surfactant self-assembly in deep eutectic solvents. *Phys. Chem. Chem. Phys.* **2018**, *20* (20), 13952−13961.
(63) Sanchez-Fernandez, A.; Leung, A. E.; Kelley, E. G.; Jackson, A. J. Complex by design: Hydrotrope-induced micellar growth in deep eutectic solvents. *J. Colloid Interface Sci.* **2021**, *581* (Pt A), 292−298.
(64) Sanchez-Fernandez, A.; Edler, K. J.; Arnold, T.; Heenan, R. K.; Porcar, L.; Terrill, N. J.; Terry, A. E.; Jackson, A. J. Micelle structure in a deep eutectic solvent: a small-angle scattering study. *Phys. Chem. Chem. Phys.* **2016**, *18* (20), 14063−73.
(65) Atri, R. S.; Sanchez-Fernandez, A.; Hammond, O. S.; Manasi, I.; Doutch, J.; Tellam, J. P.; Edler, K. J. Morphology Modulation of Ionic Surfactant Micelles in Ternary Deep Eutectic Solvents. *J. Phys. Chem. B* **2020**, *124* (28), 6004−6014.
(66) Warr, G. G.; Atkin, R. Solvophobicity and amphiphilic self-assembly in neoteric and nanostructured solvents. *Curr. Opin. Colloid Interface Sci.* **2020**, *45*, 83−96.
(67) Schick, M. J. Effect of Temperature on the Critical Micelle Concentration of Nonionic Detergents. Thermodynamics of Micelle Formation1. *J. Phys. Chem.* **1963**, *67* (9), 1796−1799.
(68) Evans, D. F.; Kaler, E. W.; Benton, W. J. Liquid crystals in a fused salt: β,γ-distearoylphosphatidylcholine in N-ethylammonium nitrate. *J. Phys. Chem.* **1983**, *87* (4), 533−535.
(69) Nandy, A.; Smiatek, J. Mixtures of LiTFSI and urea: ideal thermodynamic behavior as key to the formation of deep eutectic solvents? *Phys. Chem. Chem. Phys.* **2019**, *21* (23), 12279−12287.
(70) Elbourne, A.; Meftahi, N.; Greaves, T. L.; McConville, C. F.; Bryant, G.; Bryant, S. J.; Christofferson, A. J. Nanostructure of a deep eutectic solvent at solid interfaces. *J. Colloid Interface Sci.* **2021**, *591*, 38−51.
(71) Hammond, O. S.; Bowron, D. T.; Edler, K. J. The Effect of Water upon Deep Eutectic Solvent Nanostructure: An Unusual Transition from Ionic Mixture to Aqueous Solution. *Angew. Chem., Int. Ed.* **2017**, *56* (33), 9782−9785.
(72) Dolan, A.; Atkin, R.; Warr, G. G. The origin of surfactant amphiphilicity and self-assembly in protic ionic liquids. *Chem. Sci.* **2015**, *6* (11), 6189−6198.
(73) Prevost, S.; Gradzielski, M. SANS investigation of the microstructures in catanionic mixtures of SDS/DTAC and the effect of various added salts. *J. Colloid Interface Sci.* **2009**, *337* (2), 472−84.
(74) Kato, S.; Nomura, H.; Zieliński, R.; Ikeda, S. Ultrasonic relaxation study of the micelle—Monomer exchange process in aqueous solutions of dodecyltrimethylammonium bromide in the presence of NaBr. *J. Colloid Interface Sci.* **1991**, *146* (1), 53−62.
(75) Vlachy, N.; Jagoda-Cwiklik, B.; Vacha, R.; Touraud, D.; Jungwirth, P.; Kunz, W. Hofmeister series and specific interactions of charged headgroups with aqueous ions. *Adv. Colloid Interface Sci.* **2009**, *146* (1−2), 42−7.
(76) Kumar, A.; Venkatesu, P. Does the stability of proteins in ionic liquids obey the Hofmeister series? *Int. J. Biol. Macromol.* **2014**, *63*, 244−53.
(77) Mazzini, V.; Craig, V. S. J. Specific-ion effects in non-aqueous systems. *Curr. Opin. Colloid Interface Sci.* **2016**, *23*, 82−93.
(78) Miranda-Quintana, R. A.; Smiatek, J. Theoretical Insights into Specific Ion Effects and Strong-Weak Acid-Base Rules for Ions in Solution: Deriving the Law of Matching Solvent Affinities from First Principles. *ChemPhysChem* **2020**, *21* (23), 2605−2617.

https://doi.org/10.1021/jacs.1c04781
J. Am. Chem. Soc. 2021, 143, 14158−14168